SJMI(2018) 01;17-28

ISSN : 2635-4608

DOI http://dx.doi.org/10.31916/sjmi2018-01-2

MR Molecular Imaging Based on Magnetic Nanoparticles

Hwunjae Lee[1], SangBock Lee[2*], Geahwan Jin[2], Sergey NETESOV[3], Giljae Lee[4]

Received: 15 May 2018 / Accepted: 15 July 2018 / Published online: 1 September 2018

Abstract The development of synchronized delivery and imaging system for small interfering RNA (siRNA) is required for the clinical application of RNA interference (RNAi) in cancer treatment. In this paper, we propose a pH-responsive, magnetic nanoparticle-based siRNA delivery system that can facilitate the safe and efficient delivery and visualization of therapeutic siRNA by high resolution magnetic resonance (MR) imaging. The synthesized nanovectors were then complexed with siRNA targeting the CD44 gene via electrostatic interaction to verify the specific gene-silencing effect. The imidazolized magnetic nanovector (ImMNV) architectures developed here facilitated improved cellular internalization and exhibited a high level in vitro down regulation compared to non-imidazolized magnetic nanovectors in metastatic breast cancer cells.

Keywords : Gen Therapy, Magnetic Nanoparticles, siRNA, MR Molecular Imaging

[2*]SangBock Lee(✉) ***corresponding author***

Dept. of Radiology, Nambu University

[1]Hwunjae Lee

Bioimaging Research Team, Division of Bio-convergence Analysis, Korea Basic Science Institute (KBSI)

e-mail : yohan0410@gmail.com

[2]Geahwan Jin

Dept. of Radiology, Nambu University

e-mail : ghjin@nambu.ac.kr

Sergey NETESOV[3]

Dept. of Biotechnology , N S U

e-mail : Netesov-s@nsu.ru

[3]Giljae Lee

Department of Radiology, Nambu University, Graduate School

e-mail : korotkoff@korea.kr

I. Introduction

RNA interference (RNAi), a post-transcriptional mechanism of specific gene regulation, is a natural cellular process whereby small RNA duplexes (or small interfering RNAs; siRNAs) targeting specific genes inhibit protein production by exerting translational repression or triggering the direct

degradation of target messenger RNA (mRNA)[1][2]. With its ability to specifically and potently silence any target genes at the RNA level, RNAi affords great opportunities to lay the foundation for a breakthrough product that would be able to rapidly generate novel therapeutics[1][2]. Despite its abundant promise, however, a number of issues and challenges remain for RNAi-based therapeutics, the most import concern being the safe and effective delivery of siRNA to the cells and tissues in the body. In other words, the success of RNAi-based therapy largely depends on the rational engineering of delivery vectors that contain functionalities such as targeting moieties, stimuli-response components, and stability enhancers[3][4][5]. Synthetic materials including cationic polymers (i.e., polylysine, polyethyleneimine, polyamidoamine, poly-β-amino esters, chitosan, etc.) have been used to condense siRNA molecules, and as a backbone for further modification with functional groups (i.e., targeting ligands, stimuli-responsive linkages, etc.) or neutral charged polymers to trigger siRNA release and to substantially reduce cytotoxic effects. In either case, the delivery carrier is mainly routed to endosomes/lysosomes and experiences a decrease in pH from physiological to lysosomal pHs. The internalized siRNA molecules, therefore, should rapidly escape into the cytosol, which is regarded as the major limitation of the transfection efficiency of synthetic material-based vectors. Several strategies have been built to overcome this unavoidable step and include the incorporation of fusogenic characters (i.e., GALA peptide, imidazole, etc.) In particular, the introduction of pH-dependent imidazole residues (pKa ~6.0) into various polycations could promote the destabilization of endosomal membranes, because an imidazole ring can be easily protonated in the endosomal environment. Although imidazole-containing polymers showed reduced binding strength with siRNA due to weak positive charge density per molecule compared to free amine-containing ones, they still offer numerous interesting perspectives for the design of a promising platform for siRNA delivery. Schematic illustration of the synthesis of pH-responsive imidazolized magnetic nanovectors (ImMNV) with cationic polymer (PLI) and magnetic nanoparticles (MNPs) through the emulsion process, and the formation of ImMNV/siRNA complexes via electrostatic interaction. Schematic illustration of a rapid change in the surface charge of ImMNV in response to a reduction in pH as a result of pH-activated protonation of imidazole rings.

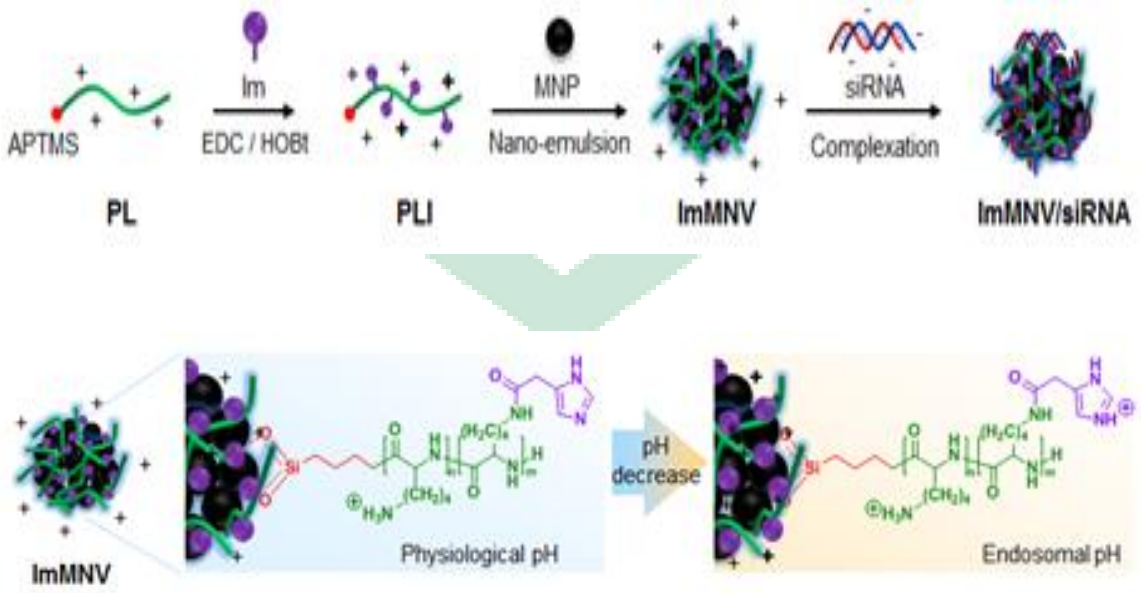

Ⅱ. Materials and methods

N6-carbobenzyloxy-L-lysine (LysZ), 4-imidazoleacetic acid, (3-aminopropyl) trimethoxysilane (APTMS), 1-ethyl-3-N,N-dimethylaminopropyl carbodiimide (EDC) hydrochloride, trifluoroacetic acid (TFA), hydrobromic acid solution (33 wt % in acetic acid) (HBr/AcOH), anhydrous tetrahydrofuran (THF), N,N-dimethylformamide (DMF), dimethylsulfoxide (DMSO), 1N sodium hydroxide (NaOH) solution, iron (III) acetylacetonate, manganese (II) acetylacetonate, 1,2-hexadecanediol, lauric acid, lauryl amine, benzyl ether, deuterium oxide (D2O), and dimethylsulfoxide-d6(DMSO-d6)werepurchasedfromSigma-Aldrich(St.Louis,MO, USA). Triphosgene was obtained from Tokyo Chemical Industry Co. (Tokyo, Japan), and 1-hydroxybenzotriazole hydrate (HOBt) was obtained from Daejung Chemicals & Metals Co. (Shiheng, Korea). n-Hexane and diethyl ether were purchased from Ducksan Scientific Co. (Seoul, Korea) and Samchun Pure Chemical Co. (Seoul, Korea), respectively. The CD44-specific siRNA (siCD44) (sense: 5′-CAGAUAGGCAAGUUUAUGA-3′, antisense: 5′-UCAUAAACUUGCCUAUCUG-3′) and negative control siRNA (siNC) (sense: 5′-CCUACGCCACCAAUUUCGU-3′, antisense: 5′-ACGAAAUUGGUGGCGUAGG-3′) were purchased from Bioneer Co. (Daejeon, Korea).

1. Fabrication of PLI-coated magnetic nanovectors (ImMNVs)

Imidazolized magnetic nanovectors (ImMNVs) as potential siRNA carriers and MR imaging agents were prepared by the nano-emulsion method. Firstly, monodisperse manganese ferrite ($MnFe_2O_4$) nanoparticles (MFs) were synthesized by the thermal decomposition of metal-organic precursors in the presence of nonpolar organic solvents.26 In detail, iron (III) acetylacetonate (2 mmol), manganese (II) acetylacetonate (1 mmol), 1,2-hexadecanediol (10 mmol), lauric acid (6 mmol), and laurylamine (6 mmol) were dissolved in 20 mL of benzyl ether. The solution was preheated to 200°C for 2 hr under an ambient nitrogen atmosphere and refluxed at 300°C for 1 hr. After cooling the reactants to room temperature, the products were purified using an excess of pure ethanol. Approximately 11-nm MFs were synthesized using the seed-mediated growth method. Twenty milligrams of the as-synthesized MFs were dissolved in 4 mL of n-hexane and subsequently added into 20 mL of DW containing 50, 100, or 200 mg of PLI (ImMNVs2.5, ImMNVs5, and ImMNVs10). After mutual saturation of the organic and aqueous phases, the mixture was ultrasonicated at 190 W for 15 min with vigorous stirring at 1,200 rpm, and stirred for 4 hr to evaporate the residual hexane. It was then collected by sequential centrifugation under three different conditions (at 15,000 rpm for 30 min, at 8,000 rpm for 15 min, and at 5,000 rpm for 15 min)

to reduce the size distribution of the polydispersed ImMNVs.

2. Characterizations of ImMNVs

The average hydrodynamic diameters and zeta potentials of the obtained ImMNVs were measured using dynamic laser scattering (ELS-Z, Otsuka Electronics, Osaka, Japan) at room temperature. Their size distributions and morphologies were observed by transmission electron microscopy (TEM, JEM-2100 LAB6, JEOL Ltd., Tokyo, Japan) at an accelerating voltage of 200 kV. The concentration of Mn plus Fe ions in the ImMNVs was measured by using inductively coupled plasma-atomic emission spectrometry (ICP-AES) analysis (IRIS Intrepid II XSP, Thermo Fisher Scientific, Boston, MA, USA). The magnetic hysteresis loop and the saturated magnetization value were obtained using a vibrating sample magnetometer (VSM, MODEL-9407, Lake Shore Cryotronics, Inc., Westerville, OH, USA) at 25°C. The amount of MFs or polymeric coatings encapsulated in ImMNVs and MNVs was measured by thermal gravimetric analysis (TGA, SDT-Q600, TA instrument, New Castle, DE, USA). The T2 relaxivity (r2) data of the ImMNV solution were obtained through magnetic resonance (MR) imaging analysis.

3. Preparation of siRNA-loaded ImMNVs

ImMNVs/siRNA complexes were formulated by briefly vortexing siRNA stock solution (10 μM) in diethylpyrocarbonate (DEPC)-treated water with the desired amount of ImMNVs, corresponding to different weight ratios of polycations to siRNA (5 to 25), for a final siRNA concentration of 0.5 μM. After mixing, the complexes were incubated for 15 min at room temperature. The siRNA condensation ability of ImMNVs was confirmed by the gel retardation assay. To compare siRNA-loading ability, siRNA was also complexed with varying amounts of MNVs. The prepared complexes were mixed with 6× HiQTM goRed (Genepole, Seoul, Korea), then loaded into a 2% agarose gel (w/v), and electrophoresed in Tris-borate-EDTA (TBE) buffer at 100 V for 20 min. The retardation of complexes was visualized by a UV lamp using a Gel Doc System.

4. Cell viability test

The cytotoxicity of ImMNVs and MNVs in breast cancer MDA-MB-231 cells was evaluated by a colorimetric assay, based on the cellular reduction of 3-(4,5-dimethylthiazoly-2)-2,5-diphenyltetrazolium bromide (MTT) (Cell Proliferation Kit I, Roche, Germany) in metabolically active cells. MDA-MB-231 cells (1×10^4 cells/well) were seeded into 96-microwell plates, incubated in RPMI 1640 medium containing 5% fetal bovine serum (FBS) and 1% antibiotics at 37°C overnight in a humidified atmosphere with 5% CO^2, and then treated with ImMNVs and MNVs containing medium with 5% FBS at various concentrations for additional 24 hr. After incubation, the yellow MTT solution was added and the formazan crystals formed were solubilized with 10% sodium dodecyl sulfate in 0.01 M HCl.

Then the relative percentage of cell viability was calculated from the formazan intensity ratio of treated to non-treated control cells and shown as an average ± standard deviation (n = 4).

5. MR imaging procedures

We performed solution and in vitro MR imaging experiments with a 1.5 T clinical MRI instrument with a micro-47 surface coil (Intera, Philips Medical Systems, Best, The Netherlands). The R2 (T2 relaxation rate, 1/T2, s^{-1}) of the ImMNV solution and ImMNV- or MNV-treated cells (1×10^7) were measured by using the Carr-Purcell-Meiboom-Gill (CPMG) sequence at room temperature with the following parameters: TR = 10 sec, 32 echoes with 12 msec even echo space, number of acquisitions = 1, point resolution of 156 × 156 μm, and section thickness of 0.6 mm. For the acquisition of T2-weighted MR images of ImMNVs solution and ImMNVs- or MNVs-treated cells, the following parameters were adopted: resolution of 234 × 234 μm, section thickness of 2.0 mm, TE = 15 msec, TR = 400 msec, and number of acquisitions = 1. The r2 ($mM^{-1}s^{-1}$) is equal to the ratio of the R2 to the ImMNV or MNV concentration.

6. Cellular uptake of ImMNVs

To prepare cellular TEM samples, MDA-MB-231 cells (1×10^6) were harvested after TrypLETM (Gibco®) treatment, washed in triplicate with blocking buffer (0.03% bovine serum albumin and 0.01% NaN^3 in phosphate-buffered solution, pH 7.4 and 10 mM) to prevent non-specific binding, and gently pelleted. Subsequently, the cells were suspended in ImMNV solution (0.46 μg/mL) and incubated for 30 min on ice and 30 min at 37°C. After incubation, the cells were washed three times with blocking buffer and fixed according to the standard fixation and embedding protocol for resin-section TEM. The sample resin blocks were trimmed and sectioned using a LEICA Ultracut UCT Ultra-microtome (Leica Microsystems Ltd., Austria). Cellular uptake of ImMNVs was also examined by the Prussian blue staining method. To stain magnetic components in MDA-MB-231 cells treated with ImMNVs (0.46 μg/mL), the cells were incubated with 2% potassium ferrocyanide in 10% HCl and then counterstained with Nuclear Fast Red (Sigma-Aldrich). Cellular internalization of the ImMNVs was observed by TEM (JEM-1011, JEOL Ltd., Tokyo, Japan) at an accelerating voltage of 80 kV and an epi-fluorescence microscope (BX51 upright microscope, Olympus, Japan).

7. In vitro transfection and quantitative reverse transcriptase-polymerase chain reaction (qRT-PCR) analysis

To measure CD44 mRNA expression levels in breast cancer cells, real time qRT-PCR analysis with internal standards was performed. Firstly, MDA-MB-231 cells (2×10^5 cells/well) were seeded in six-well plates containing 2 mL culture

medium supplemented with 10% FBS and incubated at 37°C overnight to reach 70% confluence at the time of transfection. The culture medium was then replaced with serum-free medium and 100 μL of ImMNVs or MNVs containing siCD44 or siNC (100 pmol) at a polycation/siRNA weight ratio of 1:2 was added to each well. As a control, MDA-MB-231 cells were also transfected with free siCD44 or siNC. After a 6-hr incubation, the medium was replaced with 2 mL fresh culture medium and further incubated at 37°C for 48 hr. The cells were harvested 48 hr after transfection, and total RNA was isolated from the cells with the RNeasy® Plus Mini Kit (QIAGEN, Hilden, Germany), according to the manufacturer's instructions. Complementary DNA (cDNA) was synthesized from 2 μg of total RNA using the High Capacity RNA-to-cDNA kit (Applied Biosystems®). The resulting cDNA was amplified by PCR, conducted with the QuantiMix SYBR Kit (PhileKorea Technology, Daejeon, Korea) on a real-time PCR system (LightCycler® 480 System, Roche). Primer sequences were as follows: CD44, forward 5′-CCTCTT GGCCTTGGCTTTG-3′ and reverse 5′-TCCATTGCCACTGTTGATCA-3′; GAPDH, forward 5′- GCTCTCTGCTCCTCCTGTTC-3′ and reverse 5′-TGACTC CGACCTTCACCTTC-3′. The PCR conditions were as follow: initial denaturation at 95°C for 10 min; 45 cycles of amplification at 95°C for 10 sec, at 60°C for 10 sec, and at 72°C for 10 sec. Each sample was performed in triplicate. The relative CD44 mRNA expression value was normalized to the endogenous reference gene (GAPDH) in the corresponding samples and relative to non-treated cells, and calculated by the ΔΔCt method.

8. Western blot analysis

To assess the down-regulation of the CD44 gene in MDA-MB-231 cells, the cells were harvested and lysed in cold RIPA buffer (Pierce®, Thermo Scientific) containing a protease inhibitor cocktail tablet (cOmplete Mini, Roche). The lysates were incubated at 4°C for 30 min and centrifuged at 13,000 rpm for 15 min. The supernatants were analysed for protein concentrations using the bicinchoninic acid (BCA) Protein Assay (Pierce®). Equal amounts (20 μg) of protein were subjected to electrophoresis on sodium dodecyl sulfate (SDS)-polyacrylamide gels and then transferred to a nitrocellulose blotting membrane (Amersham ™ Hybond ECL, GE Healthcare). The blotted membranes were immunostained with antibodies specific for CD44 (156-3C11, Cell Signaling Technology, Inc., USA) and GAPDH antigens (6C5, Santa Cruz Biotechnology, Inc., USA). The signals were developed by a standard enhanced chemiluminescence (ECL) method (Pierce® ECL Plus Western Blotting Substrate) according to the manufacture's protocol.

III. Results and discussion

1. Preparation of imidazolized magnetic nanovectors (ImMNVs)

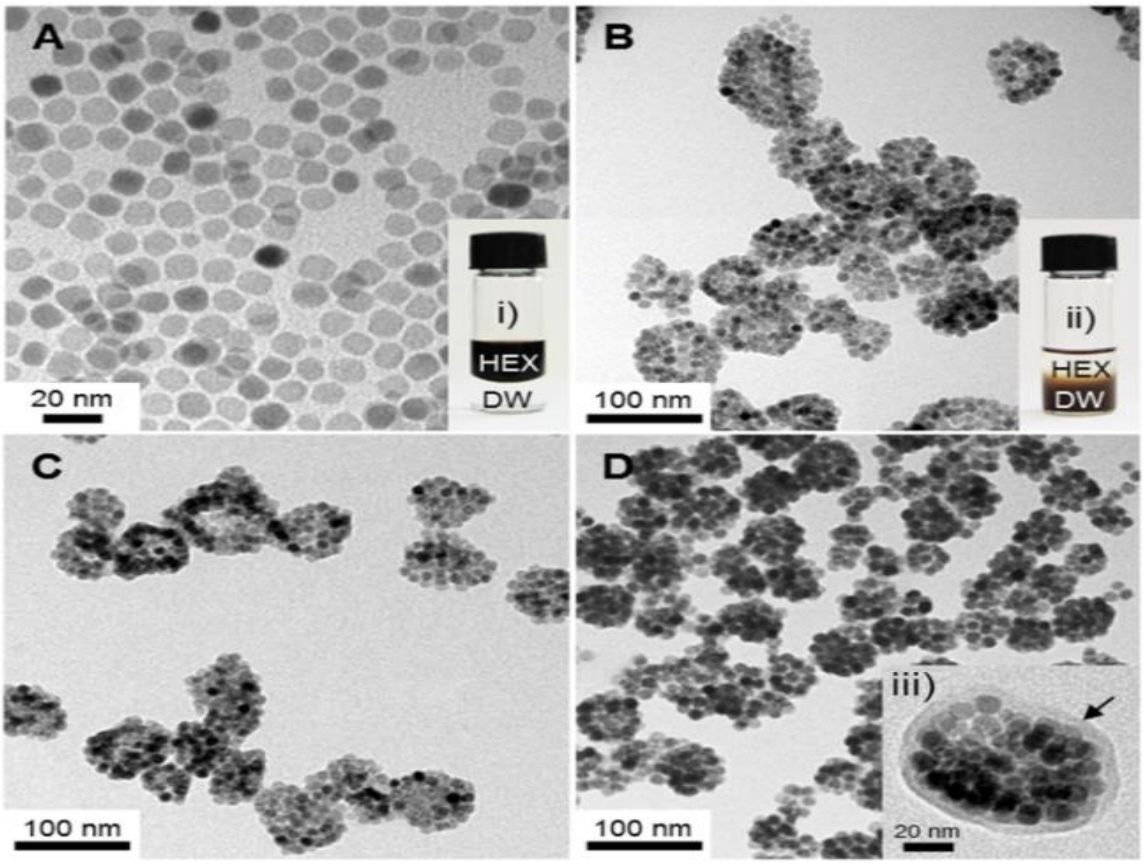

Fig. 1. TEM images of (A) lauric acid coated MFs, (B) ImMNVs2.5, (C) ImMNVs5.0, and (D) ImMNVs10.

Fig. 1. show photographs of (i) MF dispersed in hexane (HEX) and (ii) ImMNV2.5 dispersed in distilled water (DW); in (iii) the image of ImMNV10 at higher magnification indicating the surface layer is clearly visible.

Based on the obtained TEM images, MFs have a highly uniform size of 11.3 ± 1.0 nm (100 particles were measured) and the formulated ImMNVs show spherical and densely packed clusters of MFs with an average size of 61.7 ± 9.0 for ImMNV2.5, 61.3 ± 8.6 for ImMNVs5, and 49.2 ± 2.9 nm for ImMNVs10. Closer examination of a single nanoparticle in the TEM image of ImMNVs10 revealed that multiple MFs were densely clustered and covered by a thin polymeric layer (~6 nm, indicated by an arrow). Non-imidazolized MNVs (MNVs) showed heterogeneous nanoclusters with irregular forms in their TEM image and a 1.3-fold increase in hydrodynamic diameter compared with ImMNVs. suggesting that PL segments alone seem to be not sufficient to stabilize the entire surface area of MFs due to the less hydrophobicity than PLI under neutral pH conditions.

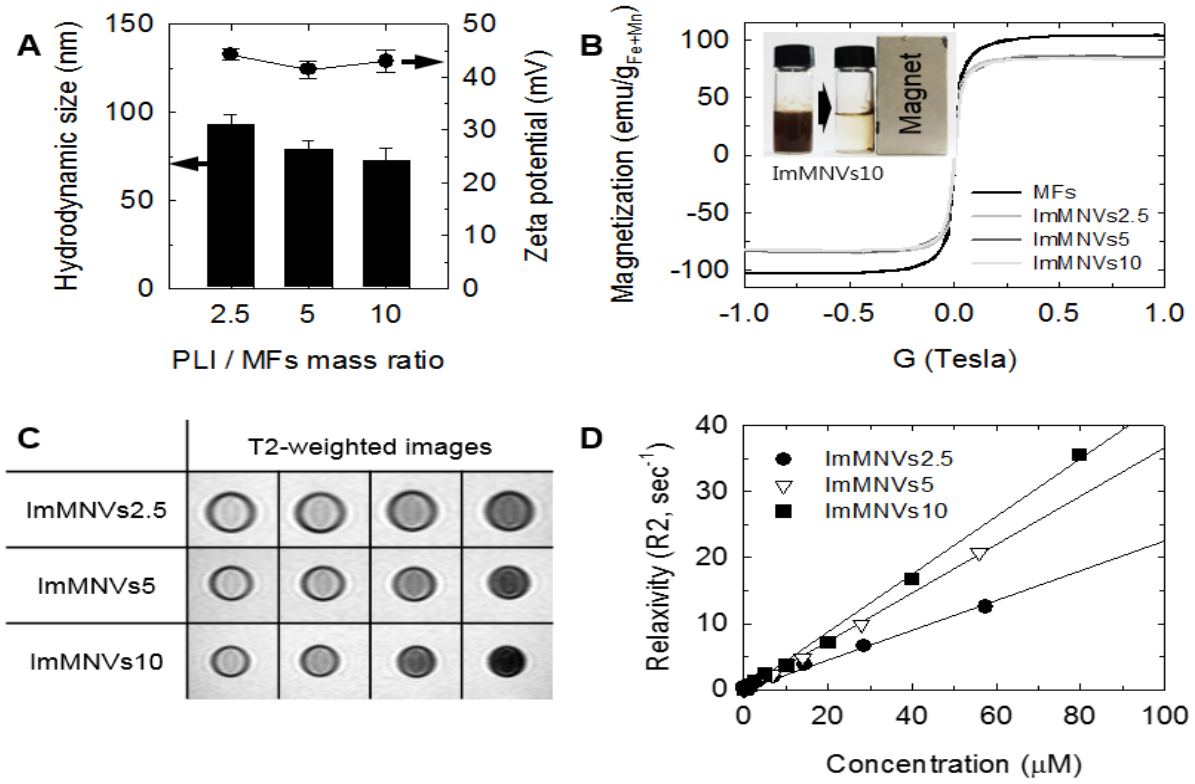

Fig. 2 Characteristics of ImMNVs as MR contrast agents.

(A) Size and zeta potential of ImMNVs prepared at various PLI/MFs mass ratios (2.5, 5, and 10). (B) Magnetic hysteresis curves of MFs and ImMNVs measured by a vibration sample magnetometer. The inset shows the magnetic sensitivity of ImMNVs10 using the Nd-Fe-B magnet. (C) T2-weighted MR images of ImMNVs in aqueous solution and (D) plots of relaxivity (R2) against ImMNV concentration.

The average hydrodynamic sizes and zeta potentials of theses ImMNVs dispersed in DI (pH 5.5) were measured using laser scattering (Fig. 2a). Overall, as the mass ratio of PLI to MFs increased from 2.5 to 10, the particle sizes slightly decreased from 93.0 ± 6.0 nm to 72.9 ± 7.1 nm, which was quite consistent with the trend in their sizes as obtained from TEM images. The hydrodynamic size of ImMNVs measured by laser scattering was larger than the value obtained from TEM because of the swelling of hydrophilic PLI polymer under the aqueous environment. It should be noted that the protonation state of the side chain of PLI changes from non-protonated imidazole to protonated imidazolinium or imidazolium in response to endosomal acidification. To assess the potential use of ImMNVs as MR imaging contrast agents, we investigated the MR images and the T2 relaxivity (R2) of variously prepared ImMNVs at different concentrations using a 1.5 T MRI instrument (Fig. 2c and 2d). As the concentration of MFs (Fe + Mn ions) in ImMNVs increased, the T2-weighted MR images were linearly darkened and the

corresponding r2 values of ImMNVs2.5, ImMNVs5, and ImMNVs10 were 224.5, 367.2, and 437.1 mM-1s-1, respectively. From these data, we demonstrated that ImMNVs10 revealed an efficient gene-loading capacity and a remarkably high MR contrast effect, and was thereby chosen for further in vitro experiments.

2. Cell viability and intracellular uptake

We next examined the in vitro differential toxicity of the prepared nanovectors using the MTT assay on the breast cancer cell line MDA-MB-231. The cells were treated with MNVs and ImMNVs at concentrations ranging from 10^{-7} to 10^{-1} mg Fe+Mn/mL and incubated for 24 hr. The cell viability in Fig. 3a showed that both MNVs and ImMNVs exhibited no significant proliferation inhibition (over 80% cell viability) up to 0.1 mg/mL with 24 hr incubation. We further evaluated the MR contrast effect of MNVs and ImMNVs in MDA-MB-231 cells using MR imaging at 1.5 T. In the T2-weighted MR images, a significant enhancement in T2 signals was obtained in ImMNVs-treated cells compared to non-treated control cells (Fig. 3b). ImMNVs were more efficiently taken up than MNVs, probably due to the higher zeta potential and r2 values of ImMNVs, as described by laser scattering and solution MR analysis. In the TEM images, the considerable amount of black clusters in MDA-MB-231 cells treated with ImMNVs implies the internalization of ImMNVs into the cytoplasm without damaging cellular structures (Fig. 4a and 4b). The images from Prussian blue staining showed similar results. Numerous blue spots, produced by the rapid exchange of electrons between Prussian blue and the ferric ions of the MFs, appeared in the intracellular region (Fig. 4c and 4d). Collectively, these results indicated that ImMNVs are suitable for use as an MR nanoprobe for versatile imaging and ultrasensitive detection at the cellular level.

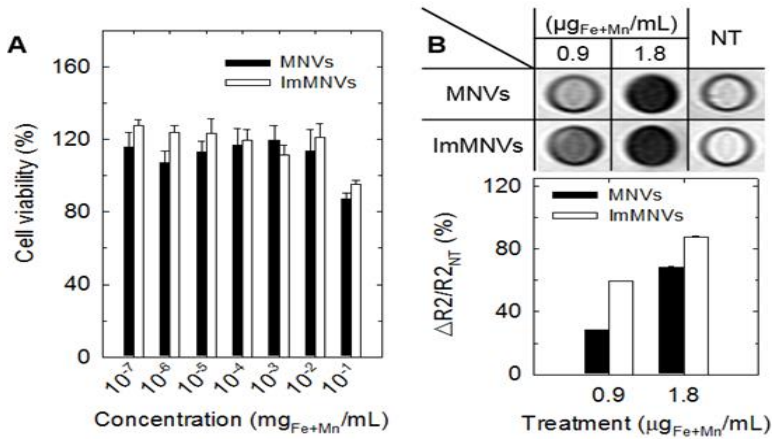

Fig. 3. (A) Cell viabilities of MDA-MB-231 cells treated with different concentrations of MNVs and ImMNVs. (B) T2-weighted MR images and the graph of ΔR2/R2NT of MDA-MB-231 cells incubated with and without MNVs and ImMNVs, respectively

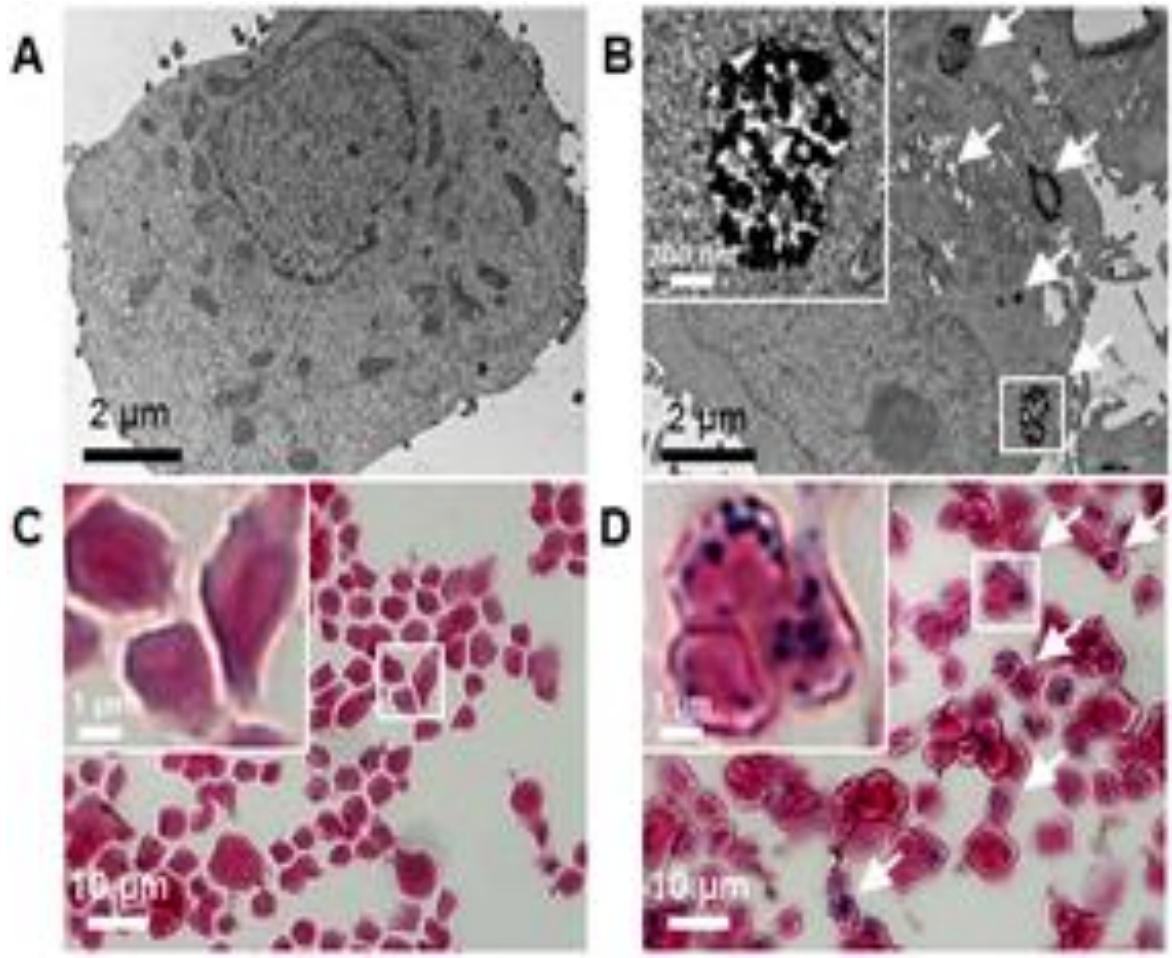

Fig. 4. Cellular TEM images and Prussian blue-stained images of MDA-MB-231 cells treated (A, C) without and (B, D) with ImMNVs. The insets show the magnified images of white boxes and the white arrows indicate the presence of ImMNVs in the cells.

3. In vitro gene silencing

To verify the potential utility of the ImMNV formulation for siRNA-based cancer therapy, the gene silencing ability of ImMNVs was investigated in metastatic breast cancer cells. MDA-MB-231 cells express high levels of the CD44 receptor, a significant prognostic biomarker of metastatic cancer, and its upregulation is highly relevant to tumor cell metastasis and invasion. Thus, these cells are appropriate for use in this study to determine therapeutic effect by knockdown of a specific gene set. In addition, this siRNA delivery system based on inorganic nanoparticles and polycations is expected to facilitate improved delivery efficiency through the process of endocytosis and an enhanced gene silencing effect by rapid endosomal escape from endosomes. Therefore, the relative expression levels of CD44 mRNA in MDA-MB-231 cells after treatment with ImMNVs containing siRNA targeting the CD44 gene (siCD44) or negative control siRNA (siNC) respectively were examined by real-time qRT-PCR analysis. For comparison, MNVs that lack

imidazole groups were complexed with siCD44 or siNC and used in the transfection experiments.

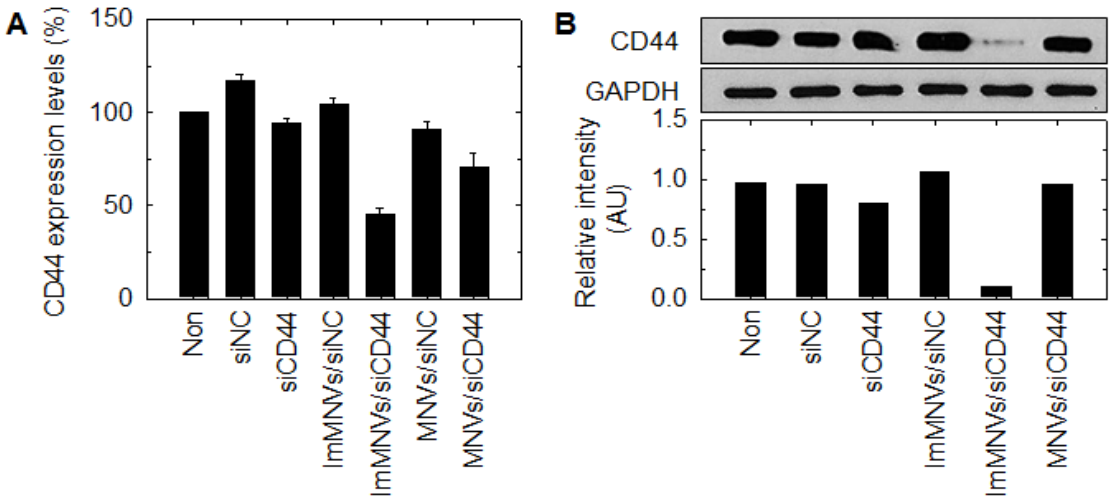

Fig. 5. Specific gene-silencing effect of MNVs/siCD44 complexes. (A) Relative expression of CD44 mRNA in MDA-MB-231 cells incubated with ImMNVs and MNVs containing siNC or siCD44, respectively. The relative mRNA expression levels (%) by qRT-PCR analysis were normalized to the mRNA level of endogenous GAPDH in the same sample. (B) Western blot analysis of CD44 from whole cell lysates of MDA-MB-231 cells treated with ImMNVs and MNVs containing siNC or siCD44 using GAPDH as a loading control. Non-treated cells were used as a negative control.

As shown in Fig. 5a, ImMNVs/siCD44 complexes clearly reduced CD44 expression by more than 54% in these cells, compared with untreated cells as well as siNC- or siCD44-treated cells. This effect is about 2-fold higher than that seen with MNVs/siCD44 complexes. In contrast, the corresponding amount (100 pmol) of siNC combined with ImMNVs did not exhibit any silencing effect, indicating target-specific gene inhibition. We further confirmed the protein expression levels of CD44 using Western blot analysis upon treatment of the cells with different conditions (Fig. 5b). As expected, CD44 protein expression had similar tendencies as observed in the qRT-PCR results. Obviously, the lowest expression of CD44 was observed in cells treated with ImMNVs, relative to other treatment groups, confirming that ImMNV-mediated intracellular delivery of siCD44 could potentially downregulate the expression of a specific gene in CD44-overexpressing cells at both the post-transcriptional and protein levels.

IV. Conclusions

In summary, we present the development and feasibility of an imidazolized magnetic nanovector (ImMNV) for the efficient delivery of therapeutic siRNA and simultaneous detection of cancer by MRI. A rationally engineered cationic polymer, PLI, as a robust stabilizer was utilized to successfully form

water-dispersible magnetic nanoclusters with cationic polymeric shells, producing a stable polyelectrolyte complex through electrostatic interaction. These ImMNVs optimized by controlling the amount of PLI in the emulsion process, showed high MR sensitivity due to their clustering effect and exhibited significant enhancement in T2 signals compared to non-imidazolized MNVs. We verified the in vitro specific gene knockdown effects of ImMNVs in MDA-MB-231 cells using both qPCR and Western blot analyses. Consequently, our proposed pH-responsive gene delivery and imaging system would be beneficial to expand research on magnetic nanoparticle-based theranostics for cancer treatment.

[Reference]

[1] A.L Jackson, S.R Bartz, J. Schelter, S.V. Kobayashi, J. Burchard, M. Mao, B. Li, G. Cavet and P.S. Linsley, "Expression profiling reveals off-target gene regulation by RNAi", *Nat. Biotechnol.*, 2003, **21**, 635-637.

[2] R. S. Kamath, A. G. Fraser, Y. Dong, G. Poulin, R. Durbin, M. Gotta, A. Kanapink, N. L. Bot, S. Moreno, M. Sohrmann, D. P. Welchman, P. Zipperlen and J. Ahringer, "Systematic functional analysis of the Caenorhabditis elegans genome using RNAi", *Nature*, 2003, **42**, 231-236

[3] D. W. Pack, A. S. Hoffman, S. Pun and P. S. Stayton, "Design and development of polymers for gene delivery", *Nat. Rev. Drug Discov.*, 2005, **4**, 581-593.

[4] S. Mura, J. Nicolas and P. Couvreur, "Stimuli-responsive nanocarriers for drug delivery", *Nat. Mater.*, 2013, **12**, 991-1003.

[5] D. Luo and W.M. Saltzman, "Enhancement of transfection by physical concentration of DNA at the cell surface", *Nat. Biotechnol.*, 2000, **18**, 33-37.

[6] Hoffman JM, Menkens AE. "Molecular imaging in cancer: future directions and goals of the National Cancer Institute". Academic radiology 2000;7(10):905-907.

[7] Nishino M, Jackman DM, Hatabu H, Janne PA, Johnson BE, Van den Abbeele AD. "Imaging of lung cancer in the era of molecular medicine". Academic radiology 2011;18(4):424-436.

[8] Kiessling F. "Science to practice: the dawn of molecular US imaging for clinical cancer imaging", Radiology 2010;256(2):331-333.

[9] Pinker K, Stadlbauer A, Bogner W, Gruber S, Helbich TH. "Molecular imaging of cancer: MR spectroscopy and beyond", European journal of radiology 2012;81(3):566-577.

[10] Guyrack Choi, Sangbock Lee, "Application and Prospects of Molecular Imaging", J. Korean. Soc. Radiol., Vol. 8, No. 3, April 2014, pp. 123~136.